ELSEVIER

Materials Chemistry and Physics 49 (1997) 184–190

MATERIALS CHEMISTRY AND PHYSICS

A study of aluminum cladding on $Ti_{50}Al_{50}$ intermetallics by liquid aluminizing

I.C. Hsu [a], S.K. Wu [a], R.Y. Lin [b]

[a] *Institute of Materials Science and Engineering, National Taiwan University, Taipei 106, Taiwan, Republic of China*

[b] *Department of Materials Science and Engineering, University of Cincinnati, Cincinnati, OH 45221, USA*

Received 1 November 1996; revised 6 January 1997

Abstract

$Ti_{50}Al_{50}$ intermetallics are successfully aluminized at 750°C by aluminum cladding. A multiple layer morphology of the aluminized coating is formed and the reaction layers are identified to be $TiAl_3$ and $TiAl_2$. During the aluminizing process, a preferred orientation along the *c* axis of DO_{22} lattice is found in the $TiAl_3$ layer and its intensity increases with increasing reaction time. A mechanism is proposed to explain this phenomenon. The $TiAl_2$ layer is formed by the reaction of the TiAl–$TiAl_3$ diffusion couple. High temperature oxidation tests reveal that the aluminized specimen shows a markedly improved oxidation resistance because of the change in the oxidation kinetics from a linear relationship to a parabolic one.

Keywords: $Ti_{50}Al_{50}$ intermetallics; Aluminum cladding; Preferred orientation of $TiAl_3$ layer; Oxidation resistance improvement

1. Introduction

TiAl intermetallics are potential high temperature materials because of their high modulus retention and good creep resistance characteristics at elevated temperatures [1,2]. However, low ductility at room temperature and insufficient oxidation resistance at high temperatures restrict their applications. Significant efforts have been made to improve the high temperature oxidation resistance but with little success [3–5]. It is well known that aluminizing is a good way to improve the surface properties of alloys, especially their oxidation and corrosion resistance [6]. For TiAl binary intermetallics, increasing the concentration of aluminum improves the oxidation resistance at high temperatures by the formation of a dense Al_2O_3 protective layer on the alloy's surface [7]. Compared with other aluminizing methods, aluminum cladding followed by liquid aluminizing in a vacuum induces higher bonding strength and produces less pollution. The main purpose of this paper is to investigate the diffusion kinetics and morphology of aluminum clad specimens of $Ti_{50}Al_{50}$ intermetallics and their high temperature oxidation resistance. The characteristics of the aluminized surface layer are also investigated.

PII S0254-0584(97)01892-0

2. Experimental procedures

A conventional tungsten vacuum arc melting technique was employed to prepare the $Ti_{50}Al_{50}$ alloy. Titanium (purity, 99.7%) and aluminum (purity, 99.97%), totalling about 80 g were melted and remelted six times in a low pressure argon atmosphere. The as-melted button was homogenized at 1050°C in a 7×10^{-5} Torr vacuum furnace for 120 h and followed by furnace cooling. The button was cut into 10 mm × 4 mm × 0.5 mm specimens and polished with #600 emery paper. In the liquid aluminizing procedure, $Ti_{50}Al_{50}$ specimens were clad with pure aluminum foil, pressed between a pair of carbon steel jaws and heated under vacuum at 750°C for various periods for aluminizing. The aluminum foil melted during heating at 750°C and reacted at the specimen's surface to form an aluminized layer. Reactions between aluminum and the carbon steel jaws were prevented by a separation layer of fire-resistant fiber textiles. Optical microscope (OM) examination, electron probe microanalysis (EPMA), X-ray diffraction analysis (XRD) and high temperature oxidation tests were conducted to investigate the structure and properties of the coating layer. Etching was conducted with Kroll's reagent (2% HF, 2% HNO_3 and 96% H_2O). XRD was performed at room temperature with a Phil-

ips diffractometer using Cu Kα radiation ($\lambda = 1.540$ Å). A JOEL JXA-8600SX EPMA apparatus was operated at 15 kV and the probe spot size was 1 μm.

3. Results

3.1. Morphology of the aluminized layer

After vacuum aluminizing at 750°C for 1, 2 and 4 h, different reaction layer thicknesses are observed as shown in Fig. 1(a), (b) and (c), respectively. The aluminized layer can be divided into several layers, i.e. the outer layer, reaction layer I, and reaction layer II. Among them, the last two constitute the primary reaction layers of aluminized $Ti_{50}Al_{50}$ intermetallics. The outer layer contains many voids and cracks. XRD and EDAX results show that this outer layer is composed of $TiAl_3$ and pure aluminum with silicon which has diffused into the sample surface from fire-resistant textile during the liquid aluminizing process. Because of the voids, cracks, and impurities, the outer layer was ineffective in protecting the substrate; therefore, for the investigation in this study, the outer layer was removed with emery paper.

Below the outer layer is reaction layer I, as shown in Fig. 1. This layer has uniform thickness, fewer cracks and more uniformly distributed pores. The thicknesses of layer I for different aluminizing time periods is about 20–150 μm. Fig. 2 shows the EPMA line scan of layer I after liquid aluminizing for 4 h. It also shows that the concentration of titanium and aluminum in this layer is almost constant. From quantitative EPMA, as indicated in Table 1, the aluminum-to-titanium ratio in this layer is found to be 3:1, and therefore the composition of reaction layer I is virtually $TiAl_3$. Evidence from XRD results discussed in Section 3.2 also confirms this conclusion.

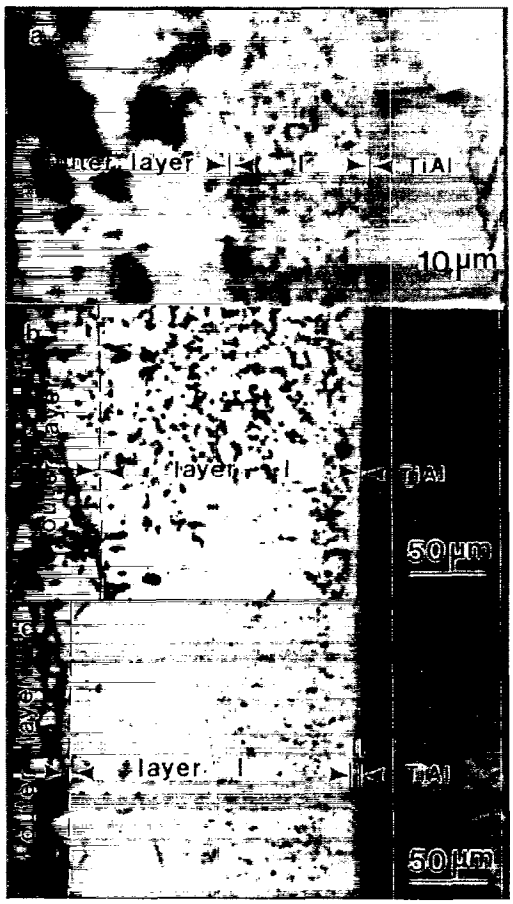

Fig. 1. Cross-sectional optical photographs of $Ti_{50}Al_{50}$ specimens aluminized at 750°C for (a) 1 h, (b) 2 h and (c) 4 h.

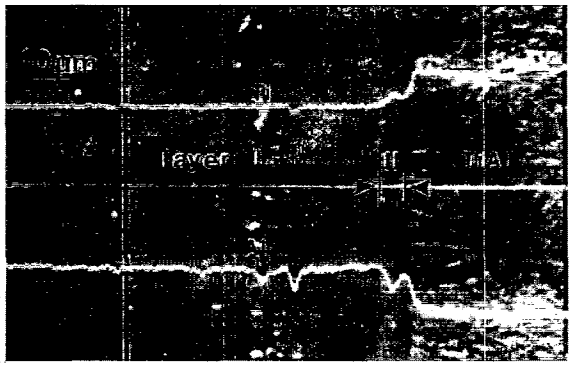

Fig. 2. EPMA line scan of $Ti_{50}Al_{50}$ specimen aluminized at 750°C for 4 h.

Table 1
EPMA quantitative analysis of the composition of layers I and II shown in Fig. 2

	Composition (at.%) (average by six points)		Standard deviation	
Layer I	Ti	Al	Ti	Al
	25.53	74.46	0.1281	0.1288
Layer II	Ti	Al	Ti	Al
	33.62	66.38	0.5832	0.5790

Between reaction layer I and the $Ti_{50}Al_{50}$ substrate, another reaction layer, reaction layer II, can be observed in Fig. 1(c) and Fig. 2. This layer reaches 5 μm in thickness after 4 h of liquid aluminizing. From the EPMA results of Table 1, the concentration ratio of aluminum to titanium in layer II is about 2:1. Therefore, its composition is suggested to be $TiAl_2$. The overall multiple layer morphology of the aluminized coating, as described above, is illustrated schematically in Fig. 3. The formation of titanium aluminides $TiAl_3$ and $TiAl_2$ is consistent with the Ti–Al equilibrium phase diagram [8].

Both titanium aluminide ($TiAl_3$ and $TiAl_2$) layers grow predominantly by the inward diffusion of aluminum into the substrate. This conclusion is made on the basis that the ratio D_{Al}/D_{Ti} in γ-TiAl is approximately 3:1, and approaches infinity in $TiAl_2$ and $TiAl_3$ [9–11]. Here, D_{Al} and D_{Ti} represent the diffusion coefficients of aluminum atoms and titanium atoms in the specified solid, respectively.

3.2. Structure identification of reaction layer I

Fig. 4 shows the XRD patterns of layer I after different aluminizing periods. The structure of this layer is clearly

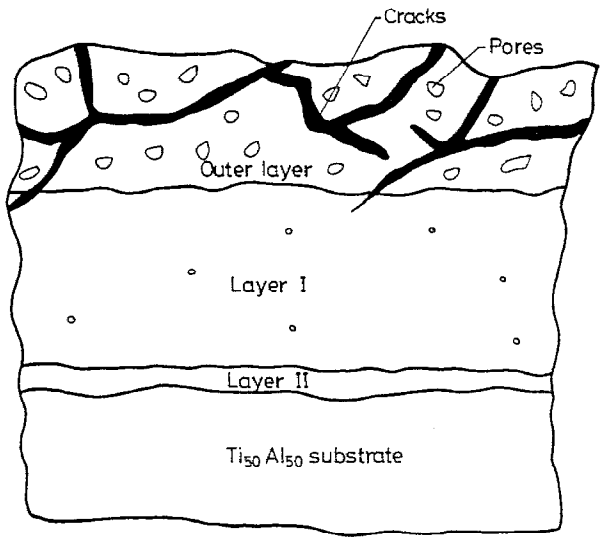

Fig. 3. Schematic diagram of the multiple aluminized layers shown in Figs. 1 and 2.

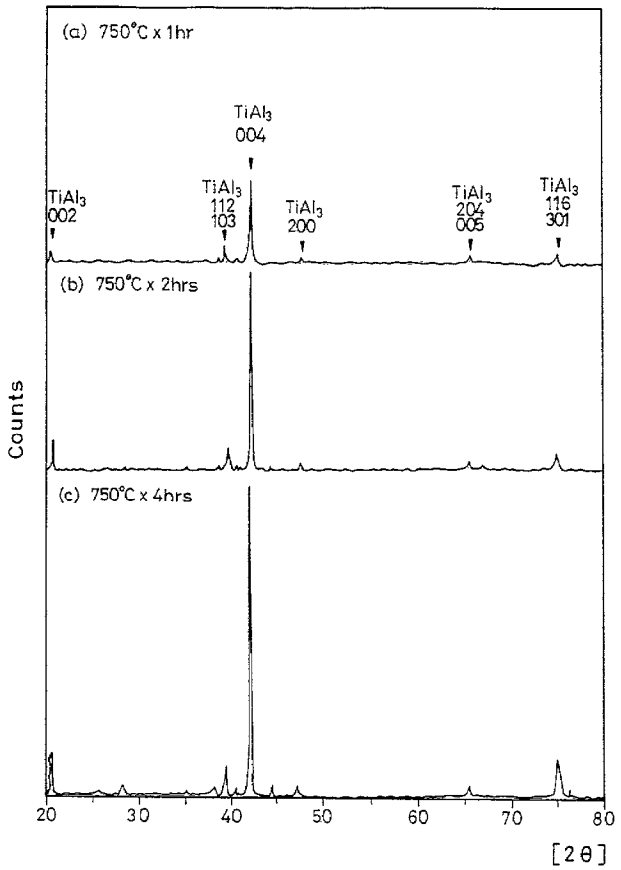

Fig. 4. XRD results of the reaction layer I aluminized at 750°C for (a) 1 h, (b) 2 h and (c) 4 h.

identified as $TiAl_3$. However, significant differences exist between the relative intensity of the diffraction patterns of the $TiAl_3$ layer and standard $TiAl_3$ DO_{22} alloy. The comparison is listed in Table 2. In Table 2, column 5 contains the angle-relative intensity data for Fig. 4(c) and column 2 gives data for standard $TiAl_3$ [12]. Here, the relative intensities of the {1 1 2} and {1 0 3} diffraction peaks in standard $TiAl_3$

Table 2
Comparison of $Ti_{50}Al_{50}$ alloy's XRD intensities obtained from this study and from the powder method

hkl	Relative intensity I/I_0			
	Powder method	1 h	2 h	4 h
002	60	70	146	166
112, 103	100	100	100	100
004	100	260	580	1163
200	60	20	40	44.8
204, 005	40	40	20	30
116	60	75	80	148
P_{004}	–	0.354	0.494	0.601

XRD pattern are the same and are referred to as 100. Compared with the relative intensities of all other diffraction peaks, the {0 0 2}, {0 0 4} and {3 0 1} diffraction peaks of Fig. 4(c) are greater than those of standard $TiAl_3$, especially for the {0 0 4} peak. This result implies that the reaction layer I has a $TiAl_3$ structure with the $c = [0\,0\,1]$ direction preferentially oriented normally to the substrate. It should be emphasized that, although the (0 0 4) and (0 0 2) planes are regarded as the same set of planes, the intensity of the {0 0 4} peak in Fig. 4 relative to that of the {0 0 4} peak in the powder is much higher than for the {0 0 2} peaks. It is well known that the relative intensity of powder pattern lines for an XRD spectra can be calculated from a structure factor F, a multiplicity factor p, a Lorentz-polarization factor L_p and a temperature factor $\exp(-2M)$, where $\exp(-2M)$ is a constant at room temperature. F and p remain constant for a specified plane in the same crystal. For a randomly oriented crystal, L_p is determined by the Bragg angle θ. However, for a crystal of preferred orientation, L_p is different from that calculated for a randomly oriented crystal owing to the radical disagreement [13]. Therefore, we suggest that the different L_p and θ used to calculate the {0 0 2} and {0 0 4} peak intensities accounts for the markedly different relative peak intensities, as shown in Table 2. The {0 0 2} and {0 0 4} are in the same set of planes, but the different L_p and θ cause the markedly different relative peak intensities. To confirm this phenomenon caused by preferred orientation, X-ray pole figure tests were conducted and the results are shown in Fig. 5. Fig. 5 indicates that the reaction layer I has a preferred orientation along the ⟨0 0 1⟩ direction. It is consistent with the above result that the $TiAl_3$ structure has the $c = [0\,0\,1]$ direction preferentially oriented normally to the substrate.

The results of Fig. 4 further indicate that the degree of preferred orientation in layer I increases for specimens with longer reaction times. We use the method of Harris [14] to calculate the extent of {0 0 4} preferred orientation, P_{hkl}, and the result is shown in Table 3:

$$P_{hkl} = \frac{I_{hkl}}{I_{r,hkl}} \Big/ \frac{1}{n}\sum \frac{I_{hkl}}{I_{r,hkl}} \qquad (1)$$

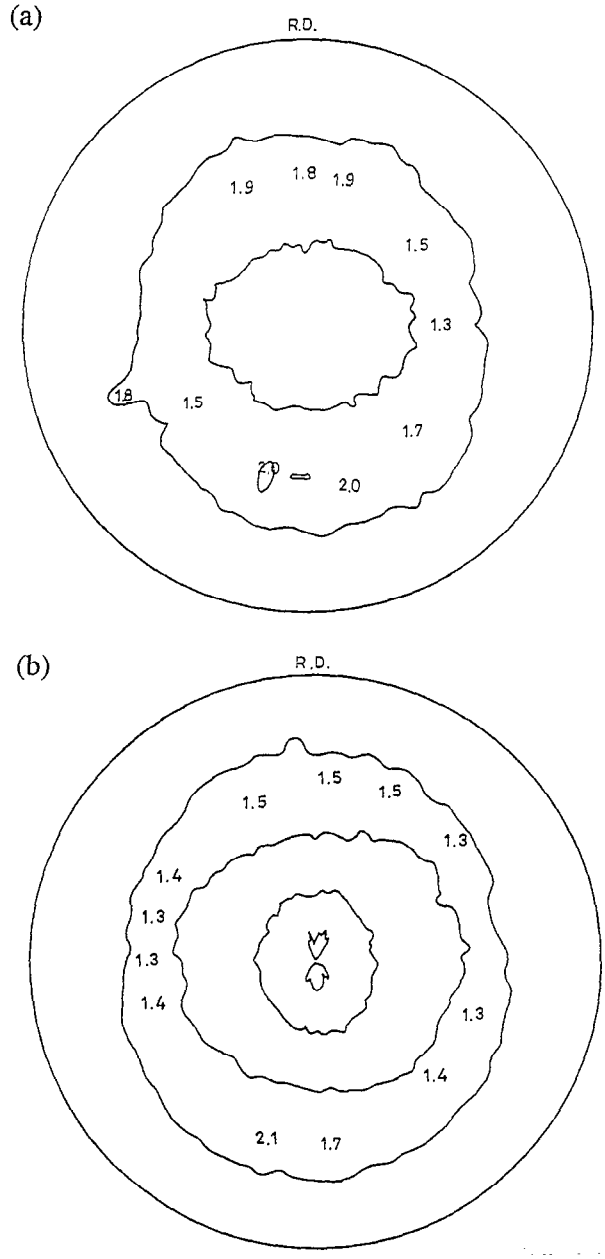

Fig. 5. (a) (1 1 1) and (b) (2 0 0) XRD pole figures of the reaction layer I aluminized at 750°C for 4 h. The numbers shown in the figures indicate pole densities in arbitary units.

Table 3
Calculation of the preferred orientation factor using the Harris method. The relative intensities of clad layer are measured from Fig. 4

hkl	Powder method	1 h	2 h	4 h
002	60	70	146	166
112,103	100	100	100	100
004	100	260	580	1163
200	60	20	40	44.8
204,005	40	40	20	30
116	60	75	80	148
p_{004}	–	0.354	0.494	0.601

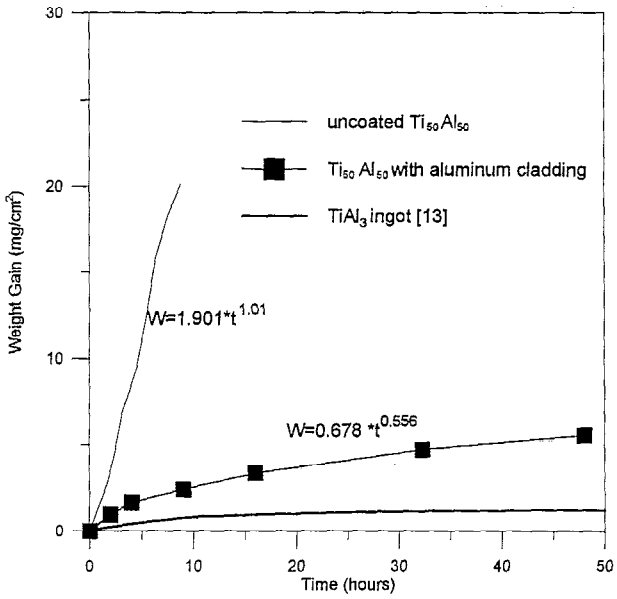

Fig. 6. Weight gain curves of 1000°C oxidation in air for specimens of $Ti_{50}Al_{50}$ ingot, $Ti_{50}Al_{50}$ alloy with aluminized and $TiAl_3$ ingot.

where P_{hkl} is the fraction of the crystals that have an $\{h\,k\,l\}$ plane, I is the relative intensity, n is the number of diffraction peaks (in Table 3, n is the peaks of $\{0\,0\,2\}$, $\{1\,1\,2\}$($\{1\,0\,3\}$) etc.) and r indicates reference diffraction patterns obtained by the powder method.

From Table 3, one can calculate that P_{004} is 0.354, 0.494 and 0.601 for 1, 2 and 4 h of aluminizing, respectively. Thus, the longer the reaction time, the higher will the relative intensity of $\{0\,0\,4\}$ be.

3.3. *High temperature oxidation test for the aluminized $Ti_{50}Al_{50}$ alloy*

In order to study the oxidation resistance of the aluminized specimens used in this study, high temperature oxidation tests were conducted. Fig. 6 is the plot of weight gain versus time for a 1000°C oxidation test in ambient air. As shown in Fig. 6, the aluminized specimen has a much better oxidation resistance than the untreated one. After exposure in air at 1000°C for 48 h, the weight gain of the aluminized specimen is below 6 mg cm^{-2}. However, the specimens that did not undergo liquid aluminizing show severe oxidation after 8 h. This fact indicates that $Ti_{50}Al_{50}$ intermetallics are effectively protected by the aluminizing. On the other hand, from Fig. 6, the oxidation resistance of aluminum clad $Ti_{50}Al_{50}$ is still inferior to that of $TiAl_3$ ingot [15]. Nevertheless, the improvement of high temperature oxidation resistance of the $Ti_{50}Al_{50}$ alloy after liquid aluminizing is still quite remarkable.

4. Discussion

4.1. *A proposed mechanism to explain the formation of preferred orientation in the $TiAl_3$ aluminized layer*

The Ti–Al binary phase diagram [8] suggests that, at 750°C, a solid–liquid reaction occurs at the interface of

$Ti_{50}Al_{50}$ substrate and molten aluminum. Because the melting point of $TiAl_3$ is higher than the aluminizing temperature, $TiAl_3$ was formed at the interface of $Ti_{50}Al_{50}$ substrate and liquid aluminum through liquid diffusion. The reaction can be written as the following equation:

$$TiAl_{(s)} + Al_{(l)} \rightarrow TiAl_{3(s)} \quad (2)$$

From the Ti–Al binary phase diagram, the solubility of titanium atoms in liquid aluminum at 750°C is about 1.5 at.%. If the titanium content exceeds 1.5 at.%, $TiAl_3$ crystals begin to nucleate at the liquid–solid interface. Once nucleation starts, crystals grow simultaneously and then touch each other to form a $TiAl_3$ layer, so an interface separates the liquid aluminum and $Ti_{50}Al_{50}$ substrate. At the same time, the growth of $TiAl_3$ grains of different crystallographic planes takes place characterized by different growing rates. Planes with the lowest surface energy grow preferentially at the highest rate, because the diffusivity either for titanium or for aluminum is a strong function of surface energy on different planes.

The long-range ordered structure of $TiAl_3$ intermetallics affects the grain growing process. As shown in Fig. 7, $TiAl_3$ has a DO_{22}-type structure, in which each unit cell contains two titanium atoms occupying the corner/center sites and six aluminum atoms occupying the face-center/edge sites. In this configuration, every aluminum atom is surrounded by four titanium atoms and eight aluminum atoms, whereas every titanium atom is surrounded by twelve aluminum atoms in the nearest neighbor sites. It is noted that aluminum diffusion in $TiAl_3$ crystal could occur without creating disorder when an aluminum atom moves to the nearest neighboring vacancy, but the movement of titanium atom to the nearest neighboring site will create an unstable Ti–Ti bond and cause disorder. At the same time, as mentioned in Section 3.1, the diffusivity of aluminum is three times faster than that of titanium in γ-TiAl. It is believed that the ratio of diffusivity of Al to Ti in $TiAl_3$ should be more than 3, because $TiAl_3$ has a much higher Al/Ti atoms ratio. The thickness increment of the $TiAl_3$ layer during the aluminizing process is virtually controlled by the diffusion of aluminum atoms. Based on this postulation, a

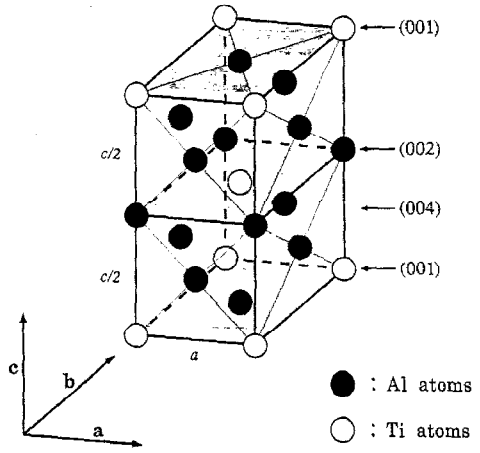

Fig. 7. Unit cell of $TiAl_3$ DO_{22} structure.

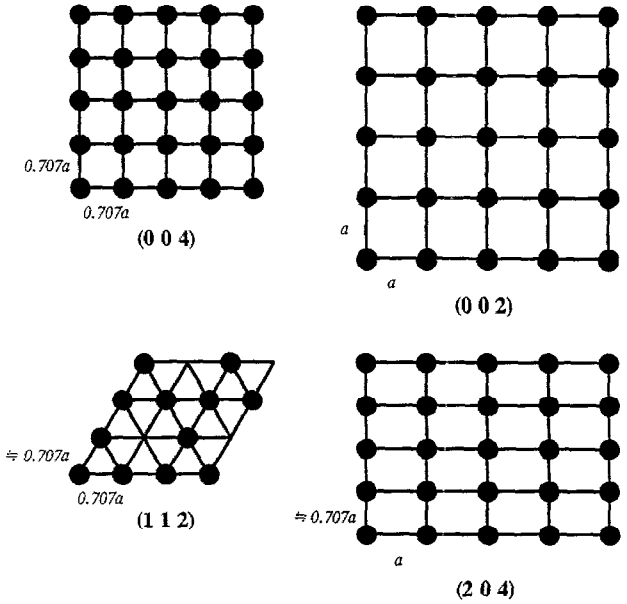

Fig. 8. Some planes of the DO_{22} structure in which only aluminum atomic sites are considered.

possible mechanism for the preferred orientation is schematically described in the following paragraph.

Fig. 8 shows some examples of atomic packing planes with the major X-ray diffraction intensities of the DO_{22} lattice, where only the atomic sites of aluminum in the DO_{22} structure are considered without the presence of titanium atoms. In Fig. 8, it can be seen that the (0 0 4) plane is the closest packed plane of the DO_{22} lattice. Therefore, aluminum atoms tend to diffuse along the (0 0 4) plane more easily than along any other plane. That is, packing of the (0 0 4) plane has a lower surface energy than any other plane. This may be the reason why $TiAl_3$ grains grow with [0 0 1] preferred orientations, as shown in Fig. 4.

This mechanism can also explain the fact that, in Fig. 4, the intensity of the (0 0 4) peak increases with increasing aluminizing time. During a longer reaction time, grains with the preferred orientation grow, while grains with other orientations gradually vanish. Oriented growth and an epitaxial relationship between liquid phase metal and metallic substrates seem quite common in intermetallics [16].

4.2. Formation of $TiAl_2$ layer

As described earlier in Section 3.1 and shown in Fig. 1, after 4 h of aluminizing at 750°C, reaction layer II is observed between reaction layer I and $Ti_{50}Al_{50}$ substrate. This layer is identified to be $TiAl_2$, which is consistent with the Ti–Al binary phase diagram [8]. Fig. 1 also shows that this layer is not thick enough to be observed in specimens aluminized for 1 or 2 h at 750°C. This means that $TiAl_2$ can be formed at the $TiAl_3$–$Ti_{50}Al_{50}$ interface only after a long reaction time. It is believed that the $TiAl_2$ layer is formed by interdiffusion between the $Ti_{50}Al_{50}$ substrate and the $TiAl_3$ reaction layer above 750°C.

Table 4
Formation energies of TiAl, $TiAl_2$ and $TiAl_3$ intermetallics [14]

	Formation energy (kJ mol^{-1})	Formation energy at 750°C (kJ mol^{-1})
TiAl	$\Delta G^f = -37445.1 + 16.79376T$	−20265
$TiAl_2$	$\Delta G^f = -43858.4 + 11.02077T$	−32584
$TiAl_3$	$\Delta G^f = -40349.6 + 10.36525T$	−29745

Thermodynamic data indicate that a $TiAl_2$ layer should be formed because of its lower formation energy. As calculated theoretically in Table 4 [17], among the formation energies of TiAl, $TiAl_2$ and $TiAl_3$, $TiAl_2$ has the largest negative value of ΔG^f at 750°C. This means that $TiAl_2$ is more stable than $TiAl_3$ and the $TiAl_2$ layer at 750°C, and it should be formed when the aluminized specimen is annealed isothermally. The difference in formation energy between the product ($TiAl_2$) and the reactant (TiAl or $TiAl_3$) provides the driving force for $TiAl_2$ formation. However, $TiAl_2$ layer cannot grow continuously because the driving force is not great enough to overcome the interfacial energy increment of the new layer. In other words, the interfacial energies of $TiAl_2$/TiAl and $TiAl_2$/$TiAl_3$ act as barriers to the formation of $TiAl_2$. A recent report also indicated that a stable phase would be absent in the diffusion zone if the driving force is not sufficient to overcome the interfacial energy increase [16]. Under this circumstance, it is suggested that $TiAl_2$ nuclei cannot grow to a distinct layer unless the aluminizing time of the specimen is extended, such as to 4 h in this study. A similar feature was reported for $TiAl_2$ growth during anneals of a TiAl–$TiAl_3$ diffusion couple at 800°C, but not at 625°C [10].

4.3. *Oxidation behavior of aluminized $Ti_{50}Al_{50}$ alloy*

The 1000°C oxidation test results shown in Fig. 6 indicate that specimens with and without aluminum cladding oxidize according to a kinetic power law. To investigate the oxidation protection of aluminized specimens, a kinetic power law is applied in terms of weight gain Δw and time t as:

$$\Delta w = kt^n \tag{3}$$

where Δw is the weight gain (mg cm^{-2}), k a rate constant, t the oxidation time (hours) and n the index of the oxidation rate. k and n can be obtained from Eq. (3) by plotting data on a log–log scale. Here, n is calculated as 1.01 (near linear) for the un-aluminized $Ti_{50}Al_{50}$ and 0.556 (near parabolic) for the aluminized specimens, as shown in Fig. 6. Linear oxidation kinetics have been observed in some other intermetallics [18]. In agreement with other authors, it can be concluded that the linear kinetics of the oxidation scale growth on the un-aluminized $Ti_{50}Al_{50}$ are controlled by grain boundary diffusion. However, the parabolic oxidation relationship has been well defined in Wagner's model [19], which shows that the oxidation scale formed on the alloy's surface acts as a protection layer to prevent further oxidation [20]. It is significant that the aluminized specimens reduced the oxidation rate at 1000°C from a linear oxidation ($n \approx 1$) to a parabolic relationship ($n \approx 0.5$), which shows that the aluminum-clad specimens exhibit a marked improvement in oxidation resistance. Using Eq. (3), setting $n = 0.5$ and replotting Fig. 6 as the weight gain versus $t^{1/2}$, we can calculate the curve's slope of the reaction rate constant as 0.55 mg cm^{-2} $h^{-1/2}$ for the aluminized specimens and 0.36 mg cm^{-2} $h^{-1/2}$ for the $TiAl_3$ ingot. The aluminized $Ti_{50}Al_{50}$ still shows slightly less oxidation protection than the $TiAl_3$ ingot. Cracks/pores existing inherently in the aluminized layer, as shown in Fig. 1, possibly account for this feature.

5. Conclusions

The study of $Ti_{50}Al_{50}$ intermetallics modified by aluminum cladding leads to the following conclusions.

1. The surface of $Ti_{50}Al_{50}$ intermetallics can be modified by aluminum cladding under a process of vacuum aluminizing. An aluminized coating of multiple layer morphology is formed. The primary reaction layers are identified to be $TiAl_3$ and $TiAl_2$.
2. The orientation of the $TiAl_3$ reaction layer grows preferentially along the c axis of DO_{22} lattice perpendicular to the surface of the specimen. This preferred orientation increases with increasing reaction time. A possible mechanism is proposed to explain this phenomenon.
3. A $TiAl_2$ layer can be formed at the interface of a $Ti_{50}Al_{50}$ substrate and a Ti_3Al reaction layer after a substantial aluminizing period. The formation of this $TiAl_2$ layer is explained in terms of a TiAl–$TiAl_3$ diffusion couple at 750°C.
4. High temperature oxidation tests indicate that the aluminized layer exhibits marked improvement in oxidation resistance. The oxidation kinetic power law of specimens subjected to liquid aluminizing is a parabolic relationship, instead of a linear oxidation as seen in specimens not subjected to liquid aluminizing.

Acknowledgements

The authors are pleased to acknowledge the financial support of this research by the National Science Council, Republic of China, under Grant No. NSC83-0405-E002-011. Also, we would like to thank Dr T.S. Chou, Steel and Aluminum R&D Department, China Steel Corporation, Kaohsiung, Taiwan, Republic of China for kindly conducting the X-ray pole figure measurements.

References

[1] H.A. Lipsitt, *Proc. Mater. Res. Soc.*, *39* (1985) 315.
[2] Y.W. Kim, *J. Mater. Sci.*, *24* (1989) 41.

[3] Y. Umakoshi, M. Yamaguchi, T. Sakagami, and T. Yamana, *J. Mater. Sci., 24* (1989) 1599.
[4] S. Taniguchi, *Bull. Jpn. Inst. Met., 31* (1992) 497. (In Japanese).
[5] S. Taniguchi, T. Shibata and K. Takeuchi, *Mater. Trans. JIM, 32* (1991) 299.
[6] M. Yoshihara, R. Tanaka, *Bull. Jpn. Inst. Met., 30* (1991) 61. (In Japanese).
[7] R. Welsch and A.I. Khveci, in T. Grobstein et al. (eds.), *Oxidation of High-Temperature Inter-metallics*, TMS, Cleveland, OH, 1988, p. 207.
[8] ASM Handbook, Vol. 3, *Alloy Phase Diagrams*, ASM International, Metal Park, OH, 1992, pp. 2–54.
[9] G.W. Goward and D.H. Boone, *Oxid. Met., 3* (1971) 475.
[10] F.J.J. van Loo and G.D. Rieck, *Acta Metall., 21* (1973) 61.
[11] F.J.J. van Loo and G.D. Rieck, *Acta Metall., 21* (1973) 73.
[12] *Powder Diffraction File*, JCPDS, Swarthmore, PA, 1983, pp. 26–39.
[13] B.D. Cullity, *Elements of X-ray Diffraction*, Addison-Wesley, New York, 2nd edn., 1978, p. 140.
[14] C.S. Barrett and T.B. Massalski, *Structure of Metals*, McGraw-Hill, New York, 3rd edn., 1980, p. 205.
[15] J.L. Smialek, *Scr. Metall., 26* (1992) 1763.
[16] F.J.J. van Loo, *Progr. Solid State Chem., 20* (1990) 47.
[17] U.R. Kattner, J.C. Lin and Y.A. Chang, *Metall. Trans., 23A* (1992) 2081.
[18] D. Dicolas-Chaubet, C. Hant, C. Picard, F. Millot and A.M. Huntz, *Mater. Sci. Eng., A120* (1989) 83.
[19] C. Wagner, *Z. Elektrochem., 63* (1959) 772.
[20] G.H. Meier, in T. Grobstein and J. Doychak (eds.), *Oxidation of High-Temperature Intermetallics*, TMS, Cleveland, OH, 1988, p. 1.